

RESEARCH ARTICLE

Applicability of heat pipes and impingement cooling for axial compressor tip clearance control: a preliminary investigation

G.M. Luz  and V. Gümmer

Technical University of Munich, Institute of Turbomachinery and Flight Propulsion, Munich, Germany

Corresponding author: G.M. Luz; Email: guilherme.luz@tum.de

Received: 16 August 2024; **Revised:** 26 February 2025; **Accepted:** 8 April 2025

Keywords: tip clearance control; axial compressor; heat pipes; impingement cooling

Abstract

This publication presents the results of a numerical analysis aimed at assessing the applicability of thermal tip clearance control (TCC) to the fore-to-last stage of a 10-stage high-pressure compressor system. The chosen geometry is representative for the HPC rear stages of a modern middle-sized turbofan, designed for large business jets and regional airliners. Simplified models for two TCC concepts were implemented, isolated and in combination: external impingement cooling and heat pipes. The analysis was performed by means of finite-element thermostructural simulations. Transient operational cycles, derived from a meanline model, along with empiric correlations for heat convection provided the required boundary conditions. Qualitative similarity to selected previous works in terms of temperature, stress and clearance evolutions was achieved. The combination of concepts demonstrated its potential as a TCC system with up to 0.45% reductions in rotor and stator clearances. Calculated heat pipe temperatures and heat fluxes were inside the estimated operational limitations. Regarding stresses, some local concentrations were observed, without significant impact in critical stress regions. A slam cycle analysis showed that, while blade rubbing remains a possibility, it can be mitigated by robust cooling control. All in all, the concept was deemed worthy of more detailed studies.

Nomenclature

Latin symbols and acronyms

A	cross-sectional area
ADP	aerodynamic design point
C_d	discharge coefficient
D	diameter
E	elasticity modulus
EGT	exhaust gas temperature
FEM	finite-element method
h	height, blade height
HP	heat pipe
HPC	high-pressure compressor
HPT	high-pressure turbine
k	thermal conductivity
L, l	length
\dot{m}	mass flow
Ma	mach number

Nu	Nusselt number
p	pressure
Pr	Prandtl number
R, r	gas constant, radius
Ra	Rayleigh number
Re	Reynolds number
s	tip gap height
t	thickness
T	temperature
TCC	tip clearance control

Greek symbols

α	convective HT coefficient
ϵ	surface emissivity
κ	isentropic exponent
σ	stress

Sub- and superscripts

a	Adiabatic
c	condensator
e	evaporator
ex	external
i	inner
is	isentropic
j	jet
o	outer
pl	plenum
s	static value
t	total value

1.0 Introduction

Improving gas path sealing has been an active field of development ever since the first gas turbine engines were designed. The impact of tip clearances on engine performance and lifespan has stirred interest on blade tip sealing techniques already from the 1960s [1]. Cooling is an effective way of doing so, given the relatively small gap sizes. The novel usage of heat pipes conceived in this work should allow effective heat removal from inner parts of the casing structure at minimal structural adaptation requirements. Inside a compressor casing, several chambers at different pressure levels and the assembly limitations of annular flanges pose a constructive challenge. Furthermore, the cooling air must come from a lower pressure region (bypass). Keeping the cool airflow external to the casing eliminates the need for designing internal sealed cavities, as well as pressurising the feedflow, which can potentially reduce overall weight and mitigate reliability issues. To the extent of the authors' knowledge, thermal TCC for compressor systems, in particular structural integration of heat pipes, is still a scarcely investigated topic.

1.1 Literature review

At first, clearance control systems were mostly investigated for the engines' hot end (HPT, LPT), given potential positive effects on component life. With tighter clearances, an engine is capable of delivering the same thrust at a smaller EGT, which in turn results in longer time spans between required maintenance rounds. In 1979, Kawecki [2] published an extensive study of turbine TCC concepts for transport and military applications. His conclusions show the positive impact of such systems over the overall

life-cycle costs of an engine. Along with blade cooling systems, turbine TCC has been established as standard in modern engines.

The development of TCC systems for the cool side of the engine (HPC) has followed somewhat different trends. It is established that tip leakage losses play a significant role on compressor efficiency and stability. One percent extra clearance can represent up to 2% less isentropic efficiency and 7.5% in surge margin [3, 4]. However, the additional costs and complexity inherent to such systems has hindered past interest on them [2]. At the time, significant performance gains were still tangible by improved aerodynamic designs. Attention to TCC modeling rose from the 1980s. Research on simple, fast-running models for tip clearance has since then been developed [5–7]. Among the goals stood correcting overall preliminary design and performance models by considering transient clearance changes. More recently, interest in TCC for HPCs has been renewed, and more extensive work was performed. Some examples are the work of Rockel et al. [8], and Schmidt et al. [9] in auxetic structures for influencing compressor tip sealings, a passive mechanical solution with limited potential. Other proposed solutions involve aerodynamically influencing tip flow so as to reduce the effective flow area, both by active inflow control [10] and recirculation [11]. On the thermal side, Horn [12] assessed air impingement for the HPC over the operational behaviour of a turbofan. Also Schmidt [13] preliminarily investigated a casing cooling design with embedded heat pipes for the HPC. Horn's work performed a very simplified analysis, with focus on the influences of clearances over the compressor operational lines by means of an idealised cylindrical casing geometry. Schmidt focused on TCC meta-modelling for fast preliminary design calculations. More detailed investigations were not performed. The survey carried out on open literature found no relevant publications concerning the application of heat pipes in axial compressors, or in other environments with similar conditions.

1.2 Objectives and text structure

The present analysis examines the thermal control concepts from a thermoelastic perspective by means of FE calculations of an elementary design of actively cooled heat pipes using a linear conduction model. It focuses on the thermal response of actively cooled heat pipes on compressor-like conditions. With less emphasis on the design integration, this first publication aims at quantitatively assessing displacements and stresses in face of localised cooling and the levels of heat flux required from the heat pipes. The influence of heat pipe pitch, axial position and cooling magnitude were investigated, and some perspectives are given regarding active control of the cooling system, especially concerning transient high-load manoeuvres.

This work starts by presenting the considered test geometry, the numerical setup and associated boundary conditions. Then, first results for a square-like test cycle are presented and a comparative discussion with selected literature sources is made to qualitatively demonstrate the model's ability of reproducing transient temperature, stress and clearance evolution trends. The influence of the different concepts, isolated and combined, is discussed and parametric studies regarding heat pipe distribution and cooling magnitude are presented. The combined concept is then tested under a high-altitude slam deceleration-acceleration cycle to assess its effect on a critical transient. Finally, conclusions and an outlook to future work wrap up the written piece.

2.0 Model setup

This section describes the setup used to characterise the representative engine operation. The workflow is summarised in Fig. 1. Details on each step are given on the subsequent subsections. Performance and meanline calculations, along with empiric correlations and physical considerations yielded the required boundary conditions (BCs) in terms of pressures, temperatures and convective heat transfer coefficients for different operational points (OPs). To reproduce transient operation, OP data was interpolated using a logarithmic function and relaxation times found in previous literature. These transient curves were then fed to the sequential thermal-structural model as appropriate BCs.

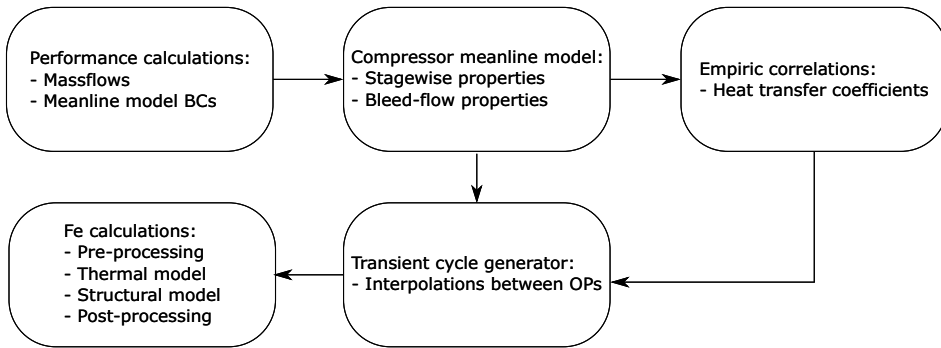


Figure 1. Model setup workflow.

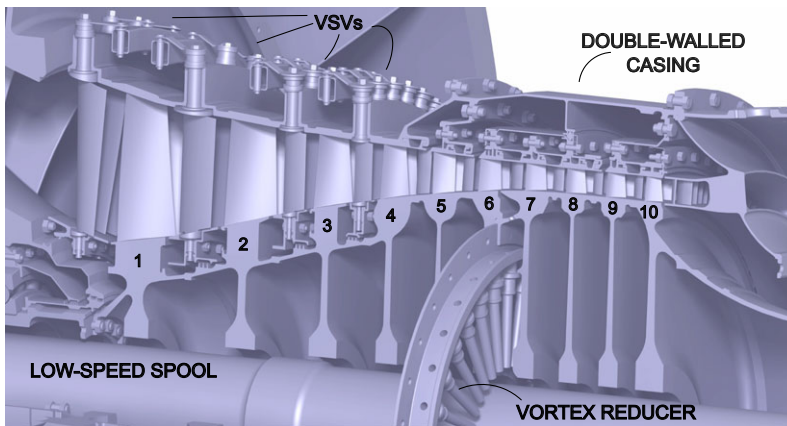


Figure 2. Cut view of representative HPC chosen for the study.

2.1 Geometry and operational points

An HPC representative geometry of a commercial twin-spool engine was selected as the study object. Similar machines are currently in-service on large business jets, as well as regional airliners with up to 80 passengers. It is displayed in Fig. 2. Modeling efforts and modifications were focused on influencing the fore-to-last stage (stage 9) following the approach taken by Rockel et al. [8] for the rotor and by Schmidt et al. [14] for the casing. The main reasons for the choice are summarised below:

- Rear compressor stages present the largest relative tip clearances, due to smaller blade heights.
- Stage 9 is far enough from the vortex reducer and from the rear cone, which allows simplifying the model to a single blisk fixed to the surrounding structure by its lateral flaps.
- The double-walled section of the casing is an assembly of annular flanges, less subject to heat-induced non-axisymmetric deformation effects (ovalisation), which eliminates the necessity of modeling the whole 360° circumference.
- Modeling the complete double-walled structure between the two external flanges allowed simplifying structural fixation, as well as considering the influences of bleed flows upon the casing thermal response.

Lattime and Steinetz's review [1] shows that axisymmetric thermal and mechanical loads are responsible for at least 70% of total clearance changes. DeCastro et al. [15] set tolerances on clearance control related to asymmetric effects at around 15% of total clearance changes. Based thereon, modeling only

axisymmetric loads and setting a minimal tolerance for clearances should suffice to adequately represent tip clearance behaviour. This also justifies the adopted simplification of a rotationally symmetric model. Only a sector of 10° was modeled. The decision to remove flange screws was based on the findings of Schmidt et al. [16]. Namely, bleed-air ports and flange screws have a negligible contribution to clearance-relevant displacements. Naturally, removing the screws and tying the flanges to one another will have an impact on local stress distributions. Those are, however, not primarily relevant for the present analysis. Finally, it was necessary to determine the material from which the structures are built. Based on Schmidt's discussion [13], INCONEL718 was chosen as the main alloy for the structure and NiCoCrAlY for the rotor coatings. Mechanical properties were taken from previous works [17–20].

Regarding operational data, little is generally available in open literature. At most, operational limits are available in engine certification sheets [21]. This information, along with guidelines adopted by previous works [13, 8] oriented the values assumed for the design point. On- and off-design data, detailed engine station data, as well as meanline data for the HPC, were then calculated by means of the commercial performance tool *GasTurb*[®]. Besides meanline properties, it was necessary to estimate the properties of relevant secondary airflows. For this purpose, the airflows were modeled as inefficient, diabatic polytropic expansions, considering the discussions of Sultanian [22]. For the transients, it was necessary to model the time evolutions of all involved variables. There is, in reality, a two-way coupling between structure and surrounding fluid flows, for which sophisticated models are required. This would be an impossible task with the available resources, so a simplified approach was adopted. Merkler et al. [5] discuss the transient behaviour of an HPC rotor disk and provide some details on the relaxation times for temperatures at different locations. Based on that, the transients were modeled by means of logarithmic functions whose coefficients depend on the prescribed relaxation times.

2.2 Numerical model and boundary conditions

The numerical model consists of a FEM implementation in the commercial software *Abaqus*[®]. Given the relatively small displacements, a one-directional coupling between the energy and the stress-displacement equations was assumed. This allows sequentially solving the transient heat transfer problem and then inputting the solution into the structural simulation, rather than solving a two-way coupled problem. The main advantages are the robustness of the solutions and the reduced computational times. The same approach was used by Rockel et al. [8] and Schmidt et al. [16]. Computations were carried out parallelised on a Unix-based high-performance computing cluster using 8 (rotor) or 16 (casing) *Intel*[®] Xeon E5-2690 v3 processors with 64GB of RAM.

The domain was discretised in fully integrated, quadratic elements. In this context, 'quadratic' translates into extra nodes added to the midpoints of edges. For a hexahedral cell, the number of nodes goes from 8 (vertices) to 20 (8 vertices + 12 edge midpoints). Additionally, the shape functions assume a quadratic polynomial form. In essence, both geometry representation and result accuracy increase, at the expense of computational effort. Element shapes and mesh structure varied according to the expected stress levels and geometry complexity. For the rotor, tetrahedral elements were used. For the casing, a mixture of structured and swept, unstructured meshing was applied. Elements were set as hexahedral. An overview of the generated meshes is provided in Fig. 3. To ensure mathematical accuracy, a grid study was performed and its results are summarised in Table 1. The three main physical parameters were compared to assess mesh convergence: *von-Mises* stresses, displacements and temperatures. They were tracked at points of interest (blade tips, rotor bore) and where highest stresses were expected (blade roots, front and rear casing flanges), throughout the whole transient cycles. The most refined meshes counted 230,591 elements, 348,108 nodes for the rotor and 222,487 elements, 1,079,165 nodes for the casing. Based on a compromise between the GIS results and computational effort, meshes R3 and C3 were chosen.

Contact modelling was required between the various parts of the casing structure. Surface-based interactions were chosen with different properties, based on the nature of contacts (screwed, mounted, rolling). The model was supplied with static pressure loads, surrounding flow temperatures, surface

Table 1. Summary of grid independence study (GIS). Percentual values were calculated as $(\Delta\phi)_{max.} = \max |1 - \phi_{finest}(t) / \phi_i(t)|$ for all tracked variables

Mesh	Elements	Nodes	$(\Delta\sigma_{Mises})_{max.} [\%]$	$(\Delta\mathbf{u})_{max.} [\%]$	$(\Delta\mathbf{T})_{max.} [\%]$
R3	160,660	245,480	<0.10	<0.10	<0.10
R2	90,495	141,401	0.33	<0.10	0.11
R1	53,378	85,252	0.40	<0.10	0.13
C3	146,039	727,955	1.11	0.21	0.10
C2	79,415	412,253	1.88	0.39	0.11
C1	47,052	254,820	3.99	0.48	0.13

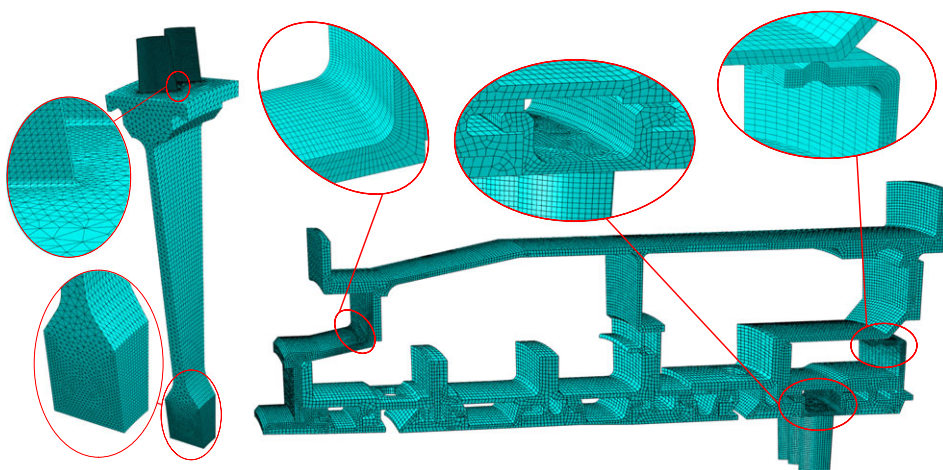


Figure 3. Reference meshes for rotor (left) and casing (right).

emissivities and convective heat transfer coefficients. The approach was based on the work of Horn [12] and Rockel et al. [8]. A comprehensive overview of the considered thermal boundary conditions is provided in Fig. 4, along with a summary of relevant correlations in Table 2. Radiation was considered by applying built-in implementations available in *Abaqus*[®]. Based on the findings of Keller et al. [23], $\varepsilon = [0.1; 0.6]$ is reasonable for INCONEL 718. Inside this range, the emissivity was set to 0.2 after preliminary simulations revealed marginal influence. This is in line with previous findings, which support the relatively small role of radiative (10%–15%) compared to convective heat transfer inside a compressor [24]. From Tirovic et al. [25] and Jalalpour et al. [26], the range for flange contact conductances in high-performance engineering applications should be about 2000–20000 W/(m²K). The conductances were set to 2000 W/(m²K), after initial calculations revealed again marginal changes in overall response for higher values.

3.0 Tip clearance control concepts

3.1 External impingement

The impingement concept was conceived based on current systems present in low-pressure turbines of typical turbofan engines. The system consists of bleeding cool air from the bypass and impinging it over the structure. A conceptual sketch of it is presented on Fig. 5. The main feature of this concept is to create a localised area of high heat transfer at the expense of little bled mass flow. Another attractive feature of external impingement is its easy integration to existing geometries without the need for major restructuring, required to isolate the various flows at different pressure levels inside the casing. In order to characterise the system, a model was created using the correlation available in Florschuetz et al. [29]

Table 2. Summary of adopted correlations for convective heat transfer over the structure

Boundary	Nu Correlation
Main annulus ^a	$0.0214Pr^{0.4} [Re^{0.8} - 100]$
Blades ^b	$\frac{0.037Re^{0.8}Pr}{1 + 2.443Re^{-0.1} [Pr^{2/3} - 1]}$
Rotor disk ^c	$6.9386 \times 10^{-6} Re_z^{1.301} \left(\frac{r}{b}\right)^{-3.523}$
Customer bleeds ^b	$0.0214Pr^{0.4} [Re^{0.8} - 100]$
Casing external surface ^b	$0.15[(1 + 2Pr^{-9/16})^{-4/9}]^{4/3} Ra^{1/3}$
Casing rear surface ^b	$0.42Pr^{0.012} Ra^{0.25} \left(\frac{h}{l}\right)^{-0.25}$
Casing rear cavity ^b	$0.2Ra^{0.25} \left(\frac{R}{r}\right)^{0.5}$

^aSource: Horn [12].

^bSource: VDI Heat Atlas [27].

^cSource: Alexiou et al. [28].

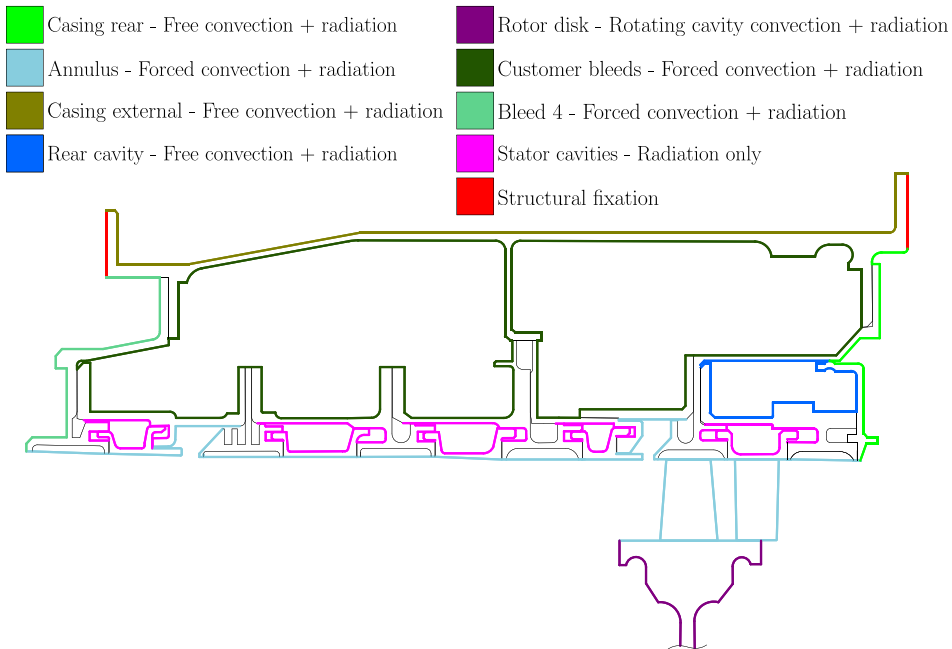


Figure 4. Meridional view of domain with considered BCs. Static pressures were also modeled for all surfaces.

for the Nusselt number and the corrections by Goodro et al. [30] for higher Mach numbers. Figure 6 schematically depicts the algorithm. Given a jet diameter (D_j) and thermodynamic state of the fluid inside the distribution box ($p_{t,pl}, T_{t,pl}$), all other relevant quantities can be calculated. That is, jet Reynolds and Mach numbers (Re_j, Ma_j), jet static pressure and temperature ($T_{s,j}, p_{s,j}$) and the jet mass flow (\dot{m}_j). Pressure losses and jet velocities are a function of the discharge coefficient, defined as the ratio of isentropic to real mass flows [31], or

$$C_d = \frac{\dot{m}_j}{\dot{m}_{j,is}} \tag{1}$$

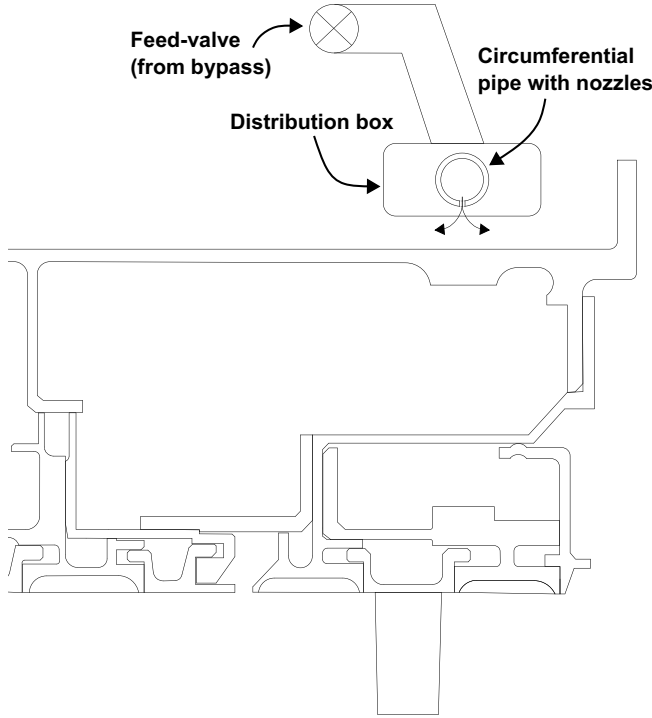


Figure 5. Conceptual design of impingement system.

where

$$\dot{m}_{j,is} = A_j \frac{p_{t,pl}}{\sqrt{RT_{t,pl}}} \left(\frac{p_{ex}}{p_{t,pl}} \right)^{\frac{1}{\kappa}} \sqrt{\frac{2\kappa}{\kappa - 1} \left[1 - \left(\frac{p_{s,j}}{p_{t,pl}} \right)^{\frac{\kappa-1}{\kappa}} \right]} \tag{2}$$

For the present work, the free design variable for the impingement system is the jet diameter. The total pressure and temperature are fixed by the available air in the bypass. Figure 7 displays the calculated impingement jet properties. The system is feasible as long as the jet static pressure is above the static pressure of the medium where the flow is impinging, which proved to be the case for all investigated diameters. From the results, smaller nozzles are more favourable. Considering the heat pipe design exposed in the next section, another restriction is that the complete condensator area is cooled by the impingement system. Therefore, the diameter is set to 3mm, also to ensure a static pressure safety margin. At this diameter, $\alpha_j=321.1 \text{ W/m}^2\text{K}$, $\dot{m}_j=0.57 \text{ g/s}$, $N_j = 130$ for $a\dot{m}_{j,total} = 74.13 \text{ g/s}$ of impingement air. Considering the estimated mass flow of 70.46 kg/s for the bypass, the amount of required bleed air lies at 0.11% and is negligible in terms of lost fan thrust.

In the FEM model, the impingement cooling is implemented as a surface boundary condition with the given temperature and heat transfer coefficient. The number of jets, as well as the surface area impacted, are determined considering that the pitchwise distribution of jets and the axial averaging length of Nu_j is equal to $5 \times D_j$.

3.2 Concentric annular heat pipes

Concentric annular heat pipes provide improved anti-gravity operation when compared to conventional designs. This is due to the extra wick area made possible by the presence of the inner pipe wall. The design considered in this work is inspired by Zhao et al. [32], who also proposed a composite wick

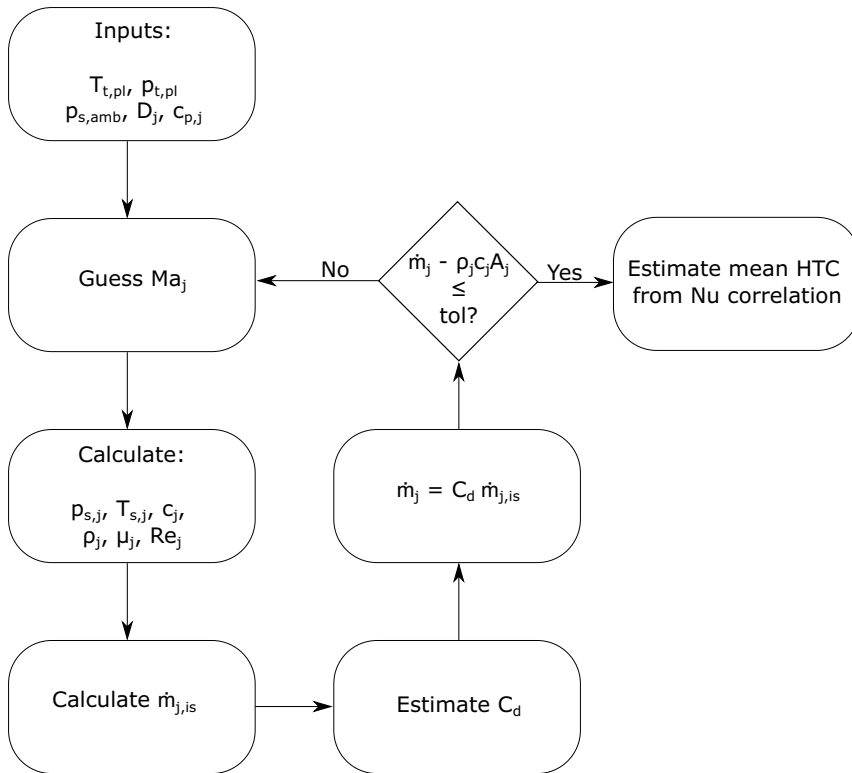


Figure 6. Impingement cooling model workflow.

design to increase the capillary limit even further for a high-temperature concentric annular heat pipe. The conceptual design of the heat pipes applied in this work is depicted in Fig. 8, along with its main dimensions, listed in Table 3.

From Noda et al. [33], a model for the screen wick properties was derived. The results were modified to include the improvements achieved by Zhao et al. [32]. Using the modelling approach described by Chi [34] and Faghri [35], and applied by Nemeč et al. [36], the operational limits of the heat pipe design were calculated. The geometric dimensions of the heat pipe were set within the limits of structural accommodation on the reference casing geometry. Material properties for the working fluid were taken from Faghri et al. [37, 38]. With all the parameters defined, it was possible to calculate the operational envelope of the heat pipe. It is displayed in Fig. 9 for the case in which the heat pipe is operating against gravity (i.e. the most unfavourable condition). The internal stresses were also estimated using a simple pressurised pipe model, as defined by Faghri [34]. Given the proposal of manufacturing the heat pipes with the same material as the casing, the estimated values are well below any material limits and were not taken as cause for concern.

The heat pipes are implemented in the FEM model as individual parts composed of two different materials. The container volume is modeled as INCONEL718, with exactly the same thermomechanical properties as the casing structure. The inner volume of the heat pipe is modeled following the approach adopted by Eisemann et al. [39]. That is, to consider the inner heat pipe material as having a small elasticity modulus (taken as $E = 10 \text{ MPa}$), a very high thermal conductivity ($k = 20000 \text{ W/m.K}$), a density and specific heat which, corresponding to the mass average of working liquid and vapor, both temperature-dependent. The thermal expansion coefficient is taken as the same as for the container. That way, the high heat flow can be simulated and non-physical effects caused by thermal expansion and mechanical stress transmission are avoided. The overall heat pipe conductivity is then mainly a function of the container

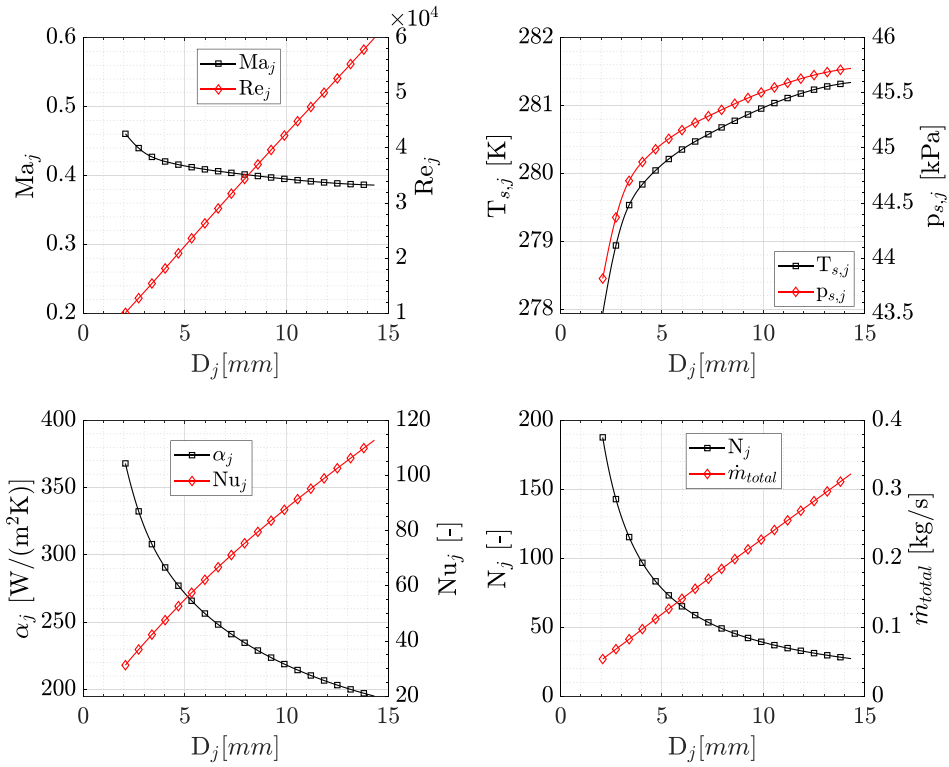


Figure 7. Impingement jet properties for fixed feedflow conditions (cruise-flight). Parameter range for which the model is valid: $Re \in [10000,60000]$; $Ma \in [0.2,0.6]$.

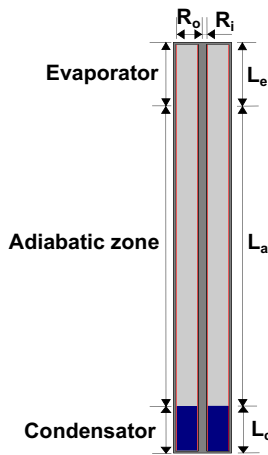


Figure 8. Conceptual design of the concentric annular heat pipe.

thickness and the wall area over which heat is transferred, which is automatically handled by the FEM solver. For the considered model, the estimated mass of one heat pipe lies at 4.7g. If they are placed circumferentially at a 5° pitch (72 units), the total added weight is 338.4g. In comparison, copper bars with the same volume would weigh in total 1.86kg, roughly 5.5 times more.

Table 3. Estimated parameters of the star-forming regions in the NGC 7,252 interacting system

Parameter	Value
R_i [mm]	0.5
R_o [mm]	4
L_e [mm]	4.3
L_a [mm]	46
L_c [mm]	7
t_p [mm]	0.5
Filling ratio	25%

Working fluid: Dowtherm®.
Wick: 400–200 screen [32].

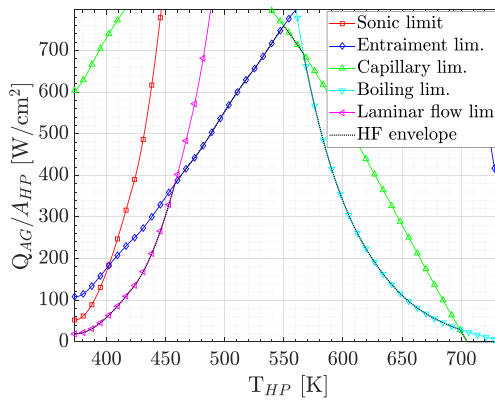


Figure 9. Heat pipe calculated operational envelope for anti-gravity operation.

4.0 Results and discussion

4.1 Square cycle analysis

Although the lack of experimental data makes proper validation an impossible task, a qualitative comparison with selected literature sources was performed. For the rotor, temperature and stress evolutions for a square cycle (IDLE-MTO-IDLE) are presented in Fig. 10. The data used by Merkler et al. [5] were used as a reference for the comparison. Given that different geometries are considered and that the reference data is not plotted in absolute terms, only trends can be compared. In general, the results are satisfactory. The stress evolutions show correct trends, with compression on the rim (red curve, lower graph in Fig. 10) during the acceleration phase, followed by stabilisation at an adequate difference between stresses in different rotor heights. The opposite behaviour is seen upon deceleration. Relatively high-bore stresses are observed, which is attributed to the fact that the rotor is simplified as a blisk. The extra mass filling the actual dovetail rails add up to the centrifugal forces being transmitted to the bore. Regarding temperature distributions, the curves are closer together than for the reference, which is due to the fact that the bleed air comes not from the compressor inlet as for the reference, but from stage 6 and is thus hotter.

For the casing structure, even qualitative comparisons in terms of temperature and stress evolutions are impractical, due to the particularities of different flange designs. Therefore, the casing response was tuned based on the resulting tip clearances. Figure 11 exhibits the calculated clearance evolution for a similar square cycle. The results of the selected literature source [6] are not reproduced here, the reader is invited to make the comparison. Referring to the deceleration from MTO to IDLE (2000s–4000s), the fast opening caused by the reduced centrifugal forces is followed by a closing caused by

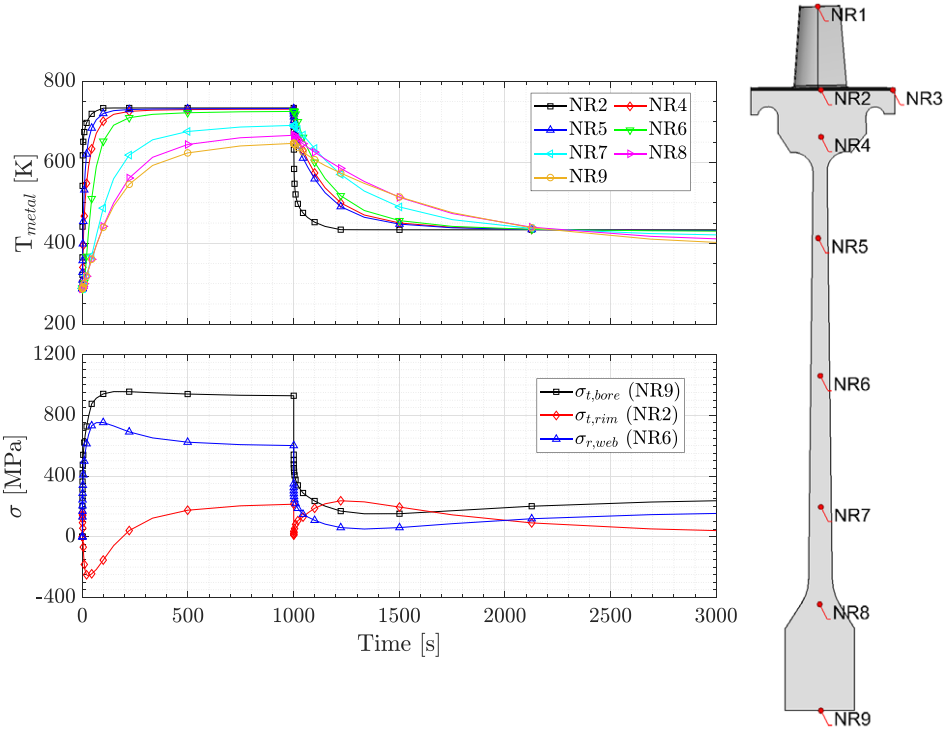


Figure 10. Temperature and stress evolutions for the rotor disk for a square test cycle (left). Reference measuring nodes (right). The time span was adjusted to match the curves displayed by Merkle et al. [5].

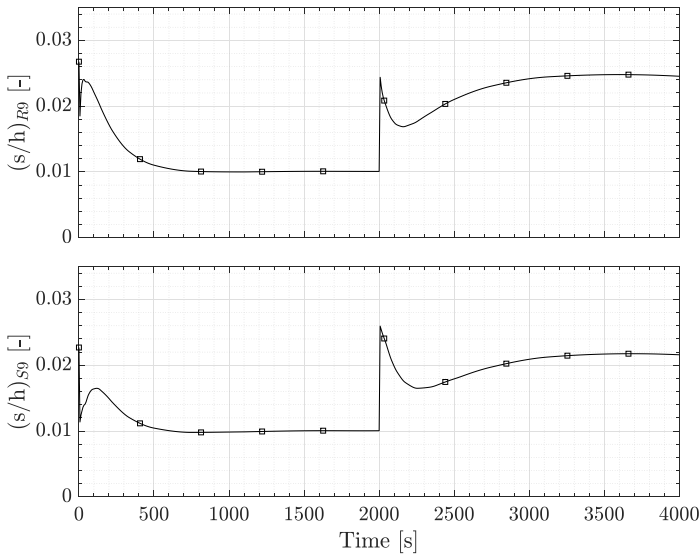


Figure 11. Calculated tip clearances in stage 9. The time span was adjusted to match the curves displayed by Schulte et al. [6].

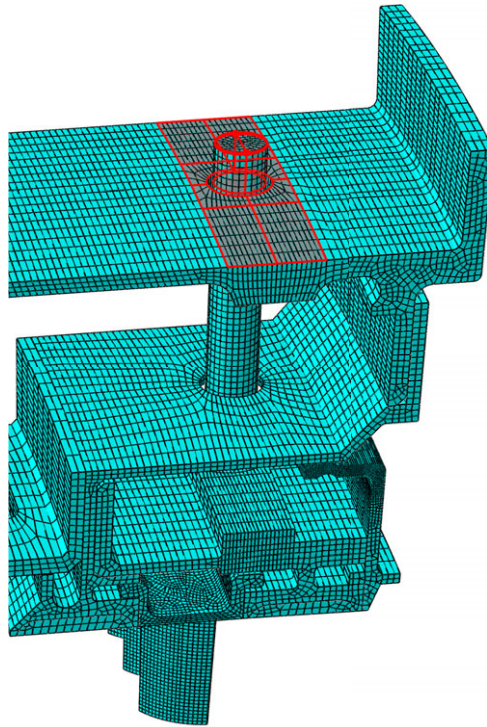


Figure 12. 10° pitch HP concept. In red, impingement BC surface.

the cooling casing. The rotor blisk, more massive, takes longer to cool. Its cooling leads to the final clearance opening towards the stationary level.

4.2 Influence of implemented TCC concepts

For evaluating the concepts, the test cycle consists of an acceleration to MTO until a stationary regime is reached, followed by a deceleration to steady ADP conditions. The whole cycle consists of 4000s, 1500s for the MTO phase and 2500s for the ADP one. The impingement system is turned on 300s after the start of the ADP phase. Figure 12 exhibits the FEM implementation of the concepts. Notice the position of the proposed heat pipe fixation in the structure, between stator 9 and rotor 10. In Fig. 13, some effects can be observed on the transient clearance curves of the different concepts. Firstly, the heat pipe decelerates the casing response to the new operational point conditions. That is reflected by a lower clearance peak after the initial pinch point at the beginning of the MTO phase (~ 100 s). Regarding ADP clearances, isolated concepts had no effect whatsoever. For the external impingement, this was expected, given the local cooling action. For the heat pipes, some appreciable effects were expected, however not seen. As it will become clear further in this work, the condenser cooling magnitude, the position and quantity of heat pipes have a defining effect over their influence. In fact, the combined concept implementation already hints at it. A very small clearance reduction was achieved for the rotor (1.69%–1.59% or 0.1%). For the stator, the effects are more pronounced (1.60%–1.31% or 0.29%). Still, a relatively small influence.

Figure 15 displays the *von-Mises* stresses for the critical region of the casing at cruise. The tendency to ‘bend’ forward due to the higher temperatures at the rear part generates the highest stresses at the front flange. For the reference, they reach 861 MPa for the MTO phase and level out at 632 MPa for cruise conditions. While the heat pipe along does not have appreciable effects over the critical stresses, the external impingement scheme actually reduces them to 494 MPa. This is due to the overall temperature reduction at the rear casing section. Naturally, there is a redistribution of stresses, not shown here, to

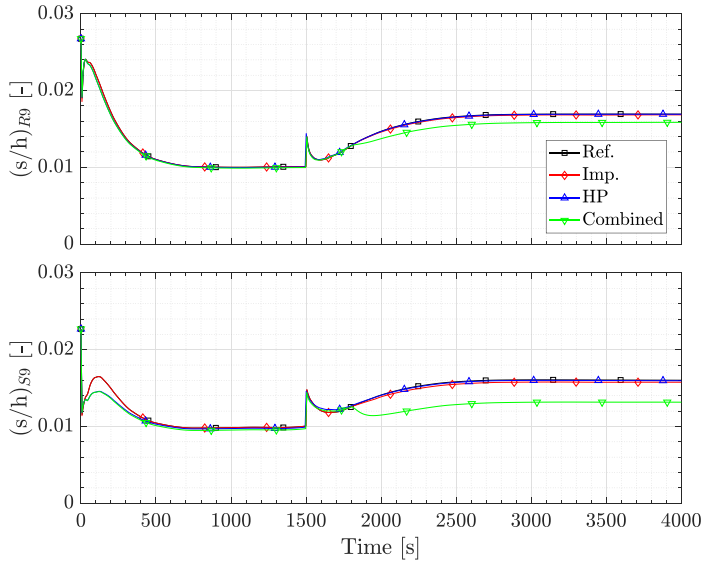


Figure 13. Clearance evolutions for implemented concepts.

other flanges at the rear part. However, the absolute stress values remain lower than the critical one. There is only one exception to this, at the bore introduced on the outer casing structure to accommodate the heat pipe. The expected geometry-induced stress concentration is enhanced by the large temperature difference caused by the impingement system, which leads to stresses up to 892 MPa at cruise. The corresponding contours are displayed in Fig. 14. A possible solution for this issue could be achieved by thermally isolating the casing structure under the impingement jets, so that the cooling effect is restricted to the HP condensators. It is to expect that any modifications on the original structure will also impact its dynamic response, mostly concerning the shifts in mass distribution created by adding the heat pipes. Aeroelastic analyses, especially concerning fluid-structure interactions, are quite sensitive to the local, unsteady flow conditions. Such level of detail is out of the scope of this preliminary investigation, and the required data is not available.

One last aspect worth mentioning relates to Fig. 9, the operational envelope of the heat pipe. At ADP, the heat pipe's temperature remains almost constant at 502 K. During the MTO phase, without cooling, it rises to 744 K. For the first condition, the maximum heat flux inside the heat pipe reaches 43.9 W/cm². For the last, it stays at 7.4 W/cm². Considering the calculated operational envelope, dry-out should occur for the MTO condition, while safe operation seems feasible for the ADP phase. Whether exposition to such high temperatures is an issue or not requires further investigation. Two main aspects here are the recuperation of dry-out and working fluid decomposition. Considering dry-out, Baraya et al. recently showed the possibility of normal operation reestablishment, with some temperature hysteresis [40]. For the intended operational point, the heat pipes can still be pushed considerably to lower temperatures to allow increased heat flux.

4.3 Influence of HP distribution

Considering the local influence of the heat pipes and the direct dependency between flange temperature and displacement (i.e. clearance), the influence of increasing the quantity of heat pipes (reducing the pitch), as well as the effects of changing their attachment position to the structure were investigated. For clarity, the FEM implementation for the 5° at the frontal position is displayed in Fig. 16. They are fixated between both vanes of stage 9, so as to have local action over the coatings of rotor 9.

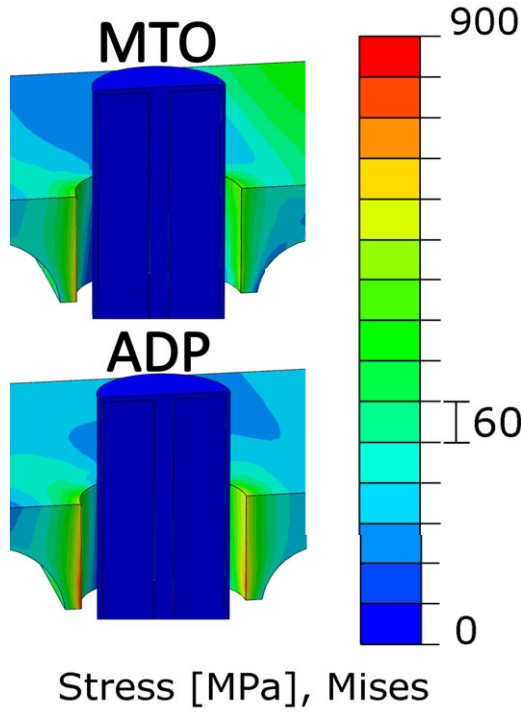


Figure 14. Stress concentration at heat pipe bores.

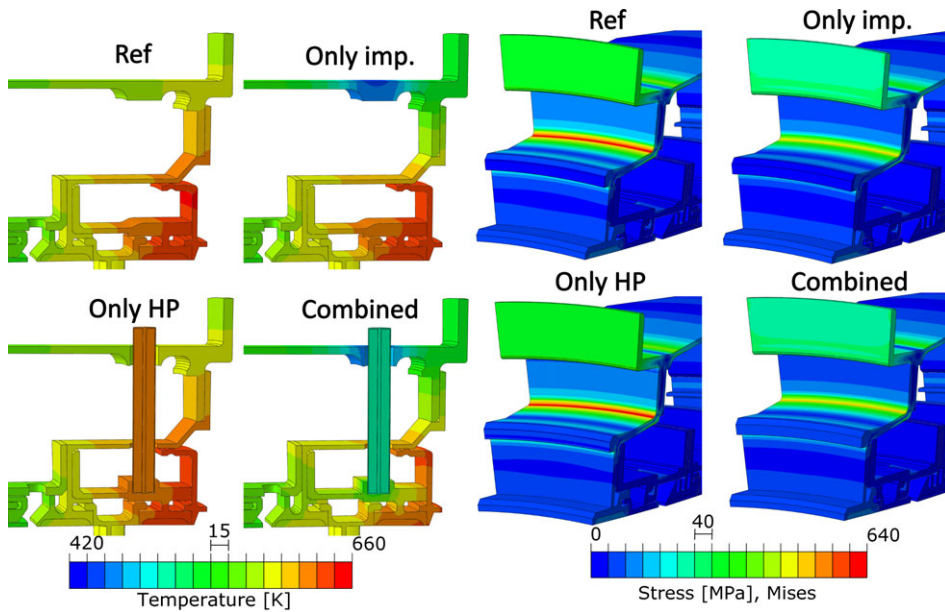


Figure 15. Temperatures at rear part of casing (left) and Von-Mises stresses in critical region (right) for the implemented concepts.

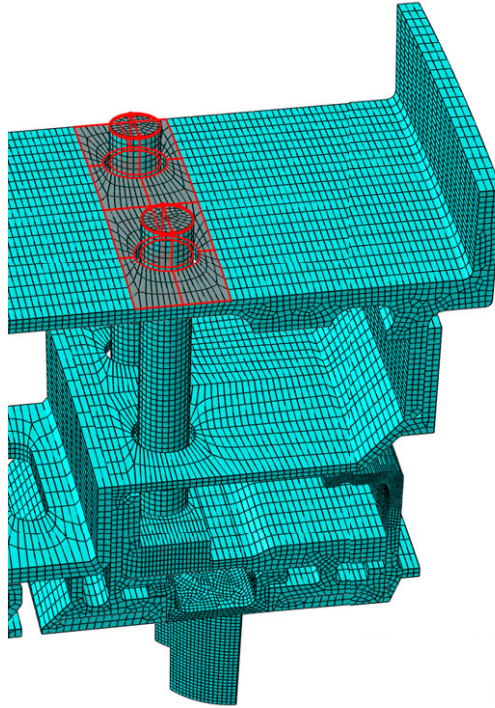


Figure 16. *5° pitch HP concept. In red, impingement BC surface.*

The obtained clearance curves are summarised in Fig. 17. The effect of positioning the heat pipes closer to the rotor is evident by comparing the respective curves (green and cyan). Rotor 9 clearances go from 1.69% to 1.50% to 1.24% considering the reference, 5° pitchwise rear and front positionings, respectively. This means a reduction in 0.29% and 0.45% clearance for the same impingement cooling. There is some penalty in the stator 9 clearances, from 1.09% to 1.17% (or 0.08% increase) when moving the heat pipes axially towards the rotor. In essence, the benefits outweigh the costs. Additionally, these results further confirm the local action of the cooling system. Regarding the quantity of heat pipes, the results are quite intuitive. The more heat pipes, the more heat transfer, the lower the temperatures and, therefore, the tighter the clearances.

Regarding stresses, the modified configuration exhibits a similar behaviour to that discussed in the previous section. The peak stresses at the casing front flange increase by little, going to about 878 MPa. The heat pipe bore holes added to cooling cause a stress concentration. However here, an additional benefit of the different heat pipe positioning becomes evident. The generally lower stress level at the front position lead to lower concentrated stress at the bores, as displayed in Fig. 18, with peak of 601 MPa on the bores for the ADP phase.

The last aspect relates to safe heat pipe operation. The discussion is similar as before, for the 10° pitch case. The operational temperatures go up to 788 K during the MTO phase, with a reduced heat flux of only 3.5 W/cm². During the ADP regime, HP temperature stabilises at 471 K with a heat flux of 37.7 W/cm². Also for this configuration, the improvement potential through enhanced condenser cooling is evident. Dry-out and working fluid decomposition during critical operation might pose an obstacle to an actual implementation.

4.4 Influence of cooling magnitude

Building on the previous discussion on the available operational envelope for cruise conditions, the impingement cooling was artificially enhanced to assess its influence over the system's response in terms

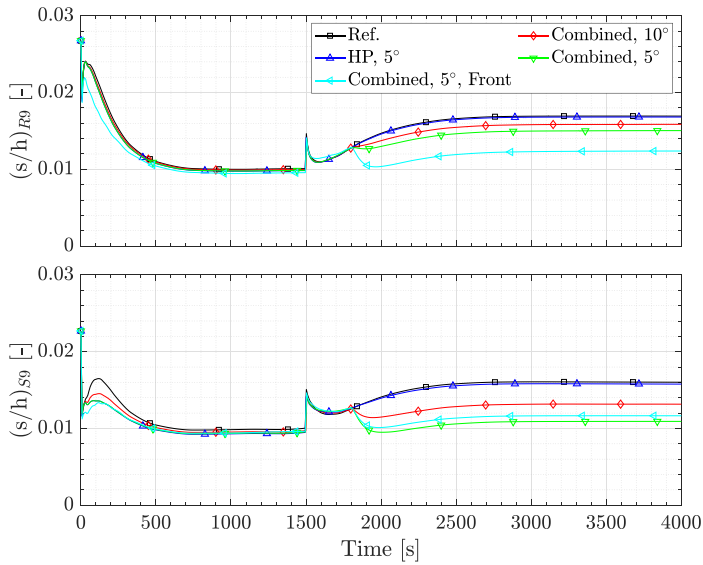


Figure 17. Clearance evolutions for different pitchwise and axial distribution of heat pipes.

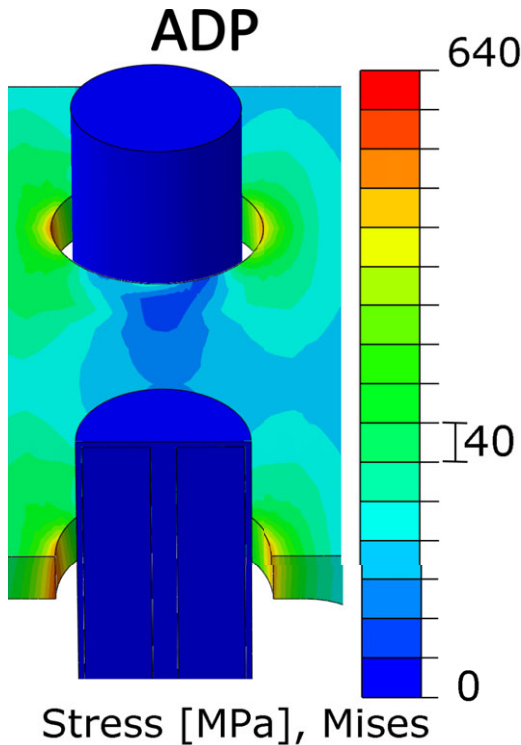


Figure 18. Stress concentration at heat pipe bores for configuration of Fig. 16.

of clearance. Figure 19 depicts the steady clearances at cruise for different impingement heat transfer coefficients. There is a slight tendency towards saturation, expected as the temperature of the heat pipes approaches that of the cooling air. The right side of Fig. 19 clarifies the tendency towards saturation. The theoretical limitation is to have a large enough cooling to equalise heat pipe and impinging air temperatures. Considering $T_j = 279.2$ K, the required magnitude of α_j would make it impractical to reach this lower limit, and already at the tested levels, the benefits become marginal when compared to

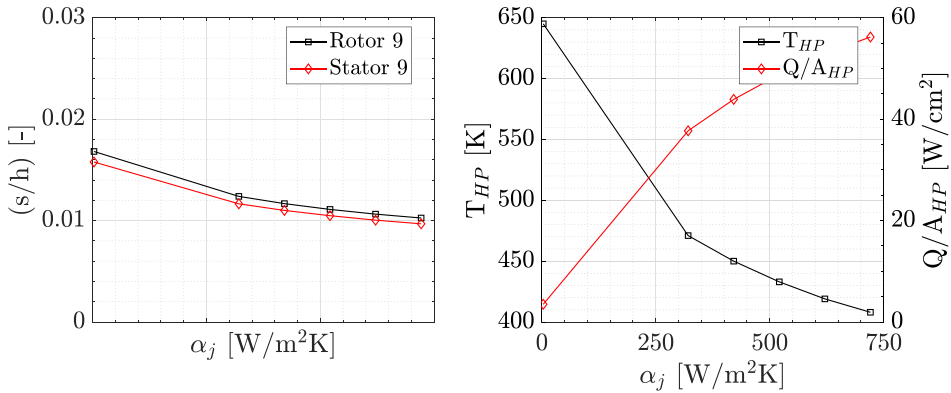


Figure 19. Variation of ADP clearances, HP temperature and max. heat flux with α_j .

the corresponding cooling enhancement. This is naturally a very simplified first assessment. Relatively simple cooling enhancement techniques, such as adding fins to the heat pipe condenser, might be worth more attention.

4.5 Clearances under slam acceleration

As a final round of assessment, the system's behaviour was analysed under a strong transient, which could potentially bring the rotor blades into rubbing danger. The test slam cycle comprises a stabilisation in cruise conditions (ADP) followed by a deceleration to high-altitude idle (HIDLE) for 100s and a consecutive acceleration to the top-of-climb condition (TCL) over another 100s, then followed by a restabilisation in ADP. Provided the impingement system is on only during the cruise phase, this transient slam cycle reflects a situation where the aircraft is required to descend for a short period and then suddenly ascend again, for example as a dodging manoeuvre to avoid incoming air traffic. Other common critical transients, such as an aborted landing, are not addressed, because the system would not be active during this flight phase. Only the combined concept with 5° HP pitch and frontal positioning was simulated (see Fig. 16). Two control cases were investigated for the impingement system. The first one was to simply leave it on during the whole transient manoeuvre. The second involved turning off the system at the start of the deceleration and turn it on after 100s of stable cruise regime. The respective results are shown in Fig. 20.

The system's influence over the transient is noticeable for the continuously on case. Pinch clearances reach a value as low as 0.63%. For the reference, the minimum clearance is 0.98%, quite close to the steady MTO one. Turning the system off improves the critical clearance in 0.24%, with a minimum of 0.87%. The stator shows a similar trend, with 0.90% for the reference compared to 0.54% for the continuous impingement case and 0.74% for the off-on case. Although conclusions on rubbing cannot be drawn at this point, the model shows that a robust control system can mitigate transient rubbing dangers by controlling the amount of impinged air and potentially its temperature.

5.0 Conclusions

This work presented a preliminary evaluation of two concepts for tip clearance control in a representative mid-sized turbofan 10-stage axial compressor. Stage 9 was the object of study. Two basic concepts, impingement cooling and heat pipes, as well as the combination of both, were assessed. A finite-element model was created, and transient thermo-structural simulations were carried out. Dynamic behaviour was not analysed. Concerning validation, qualitative similarity with selected literature results was achieved. No strict validation was possible, even though necessary, due to the lack of experimental data.

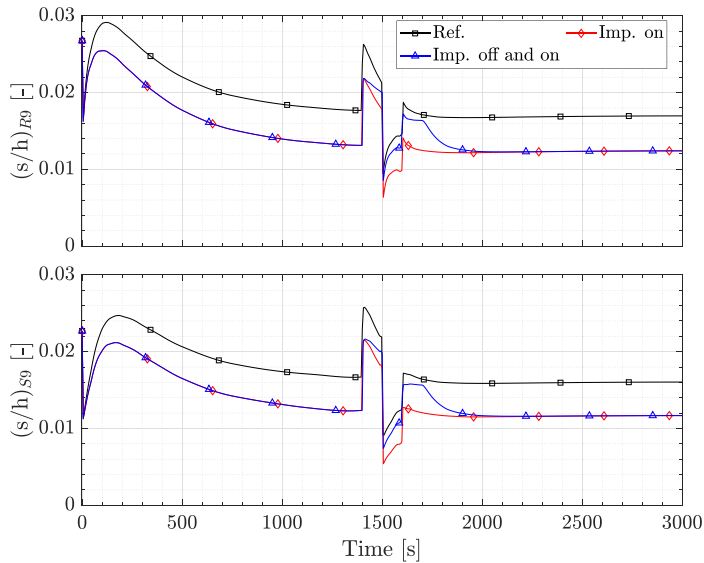


Figure 20. Clearance evolutions for high-altitude slam transient cycle.

The results demonstrate the potential of the combined impingement-heat pipe TCC concept with air supply from the bypass with no pressurisation. The best investigated configuration (5° pitchwise HP placement + impingement) reduced clearances in up to 0.45% for the rotor and 0.43% for the stator. Considering previous literature works, this could reflect in up to 0.9% polytropic efficiency gains. An analysis of the *von-Mises* stresses on the model showed some stress concentration on the holes made to accommodate the heat pipes. However, the combined system does not significantly impact the casing stress field. An artificial increase in the cooling magnitude demonstrated further clearance reduction potential, tending towards saturation, as the heat pipe temperatures decreased.

A transient slam analysis was also performed to preliminarily assess rubbing danger. Although conclusive statements cannot be made, a robust impingement control system can mitigate the severity of clearance pinch points. By simply turning impingement off as the engine decelerates and reaccelerates, 0.24% opening of the actively controlled critical clearance was achieved. In summary, the combined concept was deemed worthy of further investigations, given the promising results.

5.1 Outlook

This paper is part of a larger project aimed at assessing the potential and laying the foundations for thermal TCC in future compressor systems. Interest in such technologies anticipates issues inherent to designs with higher overall pressure ratios, i.e. larger relative clearances. Follow-up work being carried out involves detailed, reliable modeling of heat pipes to enable proper structural integration and design optimisation, in addition to closer insight on limiting phenomena such as the wick's capillary limit. The dynamic perspective must also be considered, especially concerning local shifts in mass distribution on the casing. Further ahead, a detailed model for the impingement cooling is planned, also aimed at system optimisation and control. Rig testing at representative conditions is also a requirement to properly validate numerical results. If established, actively cooled heat pipes might find a whole new high-performance application field within aeroengine compressors.

Acknowledgements. The authors would like to acknowledge the contribution of the LRZ – Supercomputing Center for providing the required computational resources for this work. A word of gratitude is extended to Mr. Pedro Henrique de Melo Casado Matos *in mem.*, Mr. Ioannis Zaimis and Mrs. Simona Rocchi for the fruitful discussions regarding the present publication.

Competing interests. The authors declare no conflict of interest of any nature upon the development and publication of this work.

References

- [1] Lattime, S. and Steinetz, B. Turbine engine clearance control systems: Current practices and future directions, in *38th AIAA/ASME/SAE/ASEE Joint Propulsion Conference & Exhibit*, AIAA 2002-3790, AIAA, Indianapolis, USA, 2002.
- [2] Kawecky, E. *Thermal Response Turbine Shroud Study*. Technical Report, Defense Technical Information Center, Fort Belvoir, Fairfax USA, 1979.
- [3] Schmücker, J. and Schäffler, A. Performance deterioration of axial compressors due to blade defects, in *Propulsion and Energetics Panel Symposium*, pp. 16.1–16.5, AGARD, Rotterdam, NE 1994.
- [4] Hupfer, A. Spalte in fluggasturbinen – ursachen, folgen und optimierungsstrategien am beispiel des turboverdichters. Habilitation, Technical University of Munich, Garching, DE, 2019.
- [5] Merkler, R., Staudacher, S., Schölch, M., Schulte, H. and Schmidt, K.-J. Simulation of clearance changes and mechanical stresses in transient gas turbine operation by a matrix method, in *41st AIAA/ASME/SAE/ASEE Joint Propulsion Conference & Exhibit*, AIAA 2005-4022, AIAA, Tucson, USA, 2005.
- [6] Schulte, H., Schmidt, K.-J., Weckend, A. and Staudacher, S. Multi-stage compressor model for transient performance simulations, in *ASME Turbo Expo: Power for Land, Sea, and Air*, pp. 185–195 ASME, Berlin, DE, 2008.
- [7] Weckend, A. Stabilitätsbetrachtungen mittels stufenweiser verdichtermodellierung in der triebwerksleistungsrechnung. Doctoral thesis, University Stuttgart, Stuttgart, DE, 2013.
- [8] Rockel, D., Weihard, S., Hachmann, A., Hupfer, A. and Kau, H.-P. Numerical investigation of an additively manufactured compressor casing: the effect of auxetic structures on the tip clearances, in *Turbo Expo: Power for Land, Sea, and Air*, GT2013-95736, ASME, San Antonio, USA, 2013.
- [9] Schmidt, T., Lorenz, J., Gümmer, V. and Hupfer, A. Structural analysis of an auxetic casing structure incorporating tip blowing casing treatment modification, *ASME Turbo Expo 2019: Turbomachinery Technical Conference and Exposition*, GT2019-91272, ASME, Phoenix, USA, 2019.
- [10] Bae, J.W., Breuer, K.S. and Tan, C.S. Active control of tip clearance flow in axial compressors, *J. Turbomach.*, May 2005, **127**, (2), pp 352–362.
- [11] Strazisar, A.J., Bright, M.M., Thorp, S., Culley, D.E. and Suder, K.L. Compressor stall control through endwall recirculation, in *Turbo Expo: Power for Land, Sea, and Air*, pp. 655–667, ASME, Vienna, Austria, 2004.
- [12] Horn, W. Verbesserung des betriebsverhaltens von turboflugtriebwerken durch aktiv geregelte verdichter. Doctoral thesis, University Stuttgart, Stuttgart, DE, 2011.
- [13] Schmidt, T. Implementierung von metamodellierungsansätzen in der vorauslegung von verdichtergehäusekonstruktionen mit fokus auf spalthaltung. Doctoral thesis, Technical University of Munich, Garching, DE, 2022.
- [14] Schmidt, T., Gümmer, V. and Konle, M. Potential of surrogate modelling in compressor casing design focusing on rapid tip clearance assessments, *Aeronaut. J.*, Sept. 2021, **125**, (1291), pp 1587–1610.
- [15] DeCastro, J. and Melcher, K. A study on the requirements for fast active turbine tip clearance control systems, in *40th AIAA/ASME/SAE/ASEE Joint Propulsion Conference & Exhibit*, AIAA 2004-4176, AIAA, Fort Lauderdale, 2004.
- [16] Schmidt, T., Gümmer, V. and Konle, M. Quantification of the effect of circumferential repeated 3d features on radial displacement of a compressor casing focusing model simplification: Part I, in *8th International Conference on Mechanics and Industrial Engineering*, p. 122.1–122.10, ICMIE, Lisbon, Portugal, 2019.
- [17] Brandt, R., Pawlowski, L., Neuer, G. and Fauchais, P. Specific heat and thermal conductivity of plasma sprayed yttria-stabilized zirconia and nial, nicr, nicral, nicrally, nicocrally coatings, *High Temperatures High Pressures (Print)*, Jan. 1986, **18**, pp 65–77.
- [18] USA Department of Defense. *Military Handbook: Metallic Materials and Elements for Aerospace Vehicle Structures*. Champaign IL, USA: USA Department of Defense, 1990.
- [19] Davis, J. *Nickel, Cobalt, and Their Alloys*. Novelty OH, USA: ASM International, 2000.
- [20] Thompson, R. and Hemker, K. Thermal expansion measurements on coating materials by digital image correlation, in *Proceedings of the SEM Conference*, pp. 1058–1067, Society of Experimental Mechanics, Springfield, USA, 2007.
- [21] European Aviation Safety Agency. *Type-Certificate Data Sheet No. E.018 for BR700–710 Engines – Rolls-Royce Deutschland GmbH*. Certification Sheet, Cologne, DE, 2022.
- [22] Sultanian, B.K. *Gas Turbines: Internal Flow Systems Modeling*, 1st ed. Cambridge, UK: Cambridge University Press, 2018.
- [23] Keller, B.P., Nelson, S.E., Walton, K.L., Ghosh, T.K., Tompson, R.V. and Loyalka, S.K. Total hemispherical emissivity of inconel 718, *Nucl Eng Design*, June 2015, **287**, pp 11–18.
- [24] Rockel, D. Zum potenzial von additiven fertigungsverfahren in zukünftigen triebwerksverdichtern. Doctoral thesis, Technical University of Munich, Garching, DE, 2015.
- [25] Tirovic, M. and Voller, G. Interface pressure distributions and thermal contact resistance of a bolted joint, *Proc. R. Soc. A: Math. Phys. Eng. Sci.*, June 2005, **461**, (2060), pp 2339–2354.
- [26] Jalalpour, M., Kim, J. and Reda Taha, M. Monitoring of l-shape bolted joint tightness using thermal contact resistance, *Exp. Mech.*, May 2013, **53**, pp 1531–1543.
- [27] Society of German Engineers (VDI). *VDI Heat Atlas*, 2nd ed. Berlin, Heidelberg, DE: Springer, 2010.
- [28] Alexiou, A., Hills, N.J., Long, C.A., Turner, A.B. and Millward, J.A. Heat transfer in high-pressure compressor gas turbine internal air systems: a rotating disc-cone cavity with axial throughflow, *Exp. Heat Transf.*, Oct. 2000, **13**, (4), pp 299–328.

- [29] Florschuetz, L.W., Truman, C.R. and Metzger, D.E. Streamwise flow and heat transfer distributions for jet array impingement with crossflow. *J. Heat Transf.*, May 1981, **103**, (2), pp 337–342.
- [30] Goodro, M., Ligrani, P., Fox, M. and Moon, H.-K. Mach number, reynolds number, jet spacing variations: full array of impinging jets. *J. Thermophys. Heat Transf.*, May 2010, **24**, (1), pp 133–144.
- [31] Ben Ahmed, F., Weigand, B. and Meier, K. Heat transfer and pressure drop characteristics for a turbine casing impingement cooling system, in *International Heat Transfer Conference*, pp. 199–212, ASME, Washington DC, USA, 2010.
- [32] Zhao, J., Ji, Y., Yuan, D., Guo, Y. and Zhou, S. Structural effect of internal composite wick on the anti-gravity heat transfer performance of a concentric annular high-temperature heat pipe, *Int. Commun. Heat Mass Transf.*, (2022), **12**, (139), p 106404.
- [33] Noda, H., Yoshioka, K. and Hamatake, T. An experimental study on the permeability of screen wicks, *JSME Int. J. Ser. B*, May 1993, **36**, (2), pp 357–363.
- [34] Chi, S. *Heat Pipe Theory and Practice: A Sourcebook*, 1st ed. Washington DC, USA: Hemisphere Publishing Corporation, 1976.
- [35] Faghri, A. *Heat Pipe Science and Technology*, 1st ed. Washington, DC, USA: Taylor & Francis, 1995.
- [36] Nemeč, P., Čaja, A. and Malcho, M. Mathematical model for heat transfer limitations of heat pipe, *Math. Comput. Model.*, Jan. 2013, **57**, (1), pp 126–136.
- [37] Faghri, A. and Zhang, Y. *Transport Phenomena in Multiphase Systems*, 1st ed. Burlington MA, USA: Elsevier, 2006.
- [38] Faghri, A., Zhang, Y. and Howell, J. *Advanced Heat and Mass Transfer*, 1st ed. Columbia MO, USA: Global Digital Press, 2010.
- [39] Eisenmann, S., Mair, M. and Hupfer, A. Structural analysis of a gas turbine disk containing heat pipes using finite element analysis, in *50th AIAA/ASME/SAE/ASEE Joint Propulsion Conference*, AIAA 2014-3840, AIAA, Cleveland, USA, 2014.
- [40] Baraya, K., Weibel, J.A. and Garimella, S.V. Heat pipe dryout and temperature hysteresis in response to transient heat pulses exceeding the capillary limit, *Int. J. Heat Mass Transf.*, Feb. 2020, **148**, p 119135.